Indonesian Journal of Pharmacy

VOL 35 (4) 2024: 599–612 | RESEARCH ARTICLE

An Integrated *in Silico-In Vitro-In Vivo* Approach for Pharmacokinetic Studies of Andrographolide Using Aqueous Extract of *Andrographis Paniculata* (Burm.F.) Wall. Ex Nees

Ghadah Faraj Aljohani[1], Nor Hafizah Zakaria[2], Fadzilah Adibah Abdul Majid[2,*], Dwi Hudiyanti[3] and Mohd Nur Nasyriq Anuar[4,]

1. Department of Chemistry, College of Science, Taibah University, PO Box 30002, Code 14177 Al-Madinah Al-Munawarah, Kingdom of Saudi Arabia
2. Institute of Climate Adaptation and Marine Biotechnology, Universiti Malaysia Terengganu, 21030 Kuala Nerus, Terengganu, Malaysia
3. Department of Chemistry, Faculty of Science Mathematics, Diponegoro University, Semarang, Indonesia
4. Discipline of Basic Health Sciences, Pharmacology and Toxicology, Faculty of Pharmacy, Universiti Sultan Zainal Abidin, 22200, Besut, Terengganu, Malaysia

Article Info

Submitted: 31-03-2-24
Revised: 01-07-2024
Accepted: 18-07-2024

*Corresponding author
Fadzilah Adibah Abdul Majid

Email:
f.adibah@umt.edu.my

ABSTRACT

Andrographis paniculata is an herbal plant that has been used traditionally for decades to treat a wide range of diseases. To this date, no research on the integration of *in silico, in vitro*, and *in vivo* pharmacokinetics (PK) has been documented on andrographolide (AG), the primary bioactive compound in *A. paniculata.* In this study, we employed an *in silico* approach to predict the physicochemical properties, metabolism, and toxicity of AG. PK properties were validated using *in vitro* assays and further tested in Wistar rats. Based on *in silico* prediction, AG was demonstrated to be a soluble, permeant, and lipophilic drug. AG was regarded as a non-mutagenic and non-carcinogenic drug with a low risk of oral absorption. *In vitro* assays showed that AG was stable at all pH levels tested, had a high equilibrium solubility, and moderately stable in the mouse plasma. AG was also permeant across the Caco-2 monolayer with P_{app} values of 9.627×10^{-6} cm/s (apical) and 18.1×10^{-6} cm/s (basolateral). It had a stable metabolism in the liver microsomes and did not have any inhibitory effects on the enzymes CYP2C8, CYP2C19, CYP2D6, or CYP3A4 (MDZ). Based on *in vivo* results, the volume of distribution and clearance were both high, with a short elimination half-life (0.17 ± 0.0 h) contributing to the low oral bioavailability (~2%). Rapid oral absorption was shown with T_{max} of 0.25 h. Our data revealed promising drug-like properties of AG, and its pharmacokinetics profiles support its potential in developing andrographolide-based products from natural resources.

Keywords: andrographolide; herbal drug; *in silico*; pharmacokinetics

INTRODUCTION

Andrographis paniculata (Burm.f.) Nees (family Acanthaceae) commonly called "Hempedu bumi" and "King of bitter" is widely distributed in South Asian countries such as Indonesia, Malaysia, Thailand, and China. It has long been used traditionally in treating sore throat, fever, and snake bites as well as in reducing inflammation and allergies (Ibrahim *et al.,* 2020). This herb is also extensively studied to prevent the occurrence of non-communicable diseases such as metabolic and cardiovascular disorders (Yoopan *et al.,* 2007; Nugroho *et al.*, 2013). Traditional knowledge has contributed to the majority of modern drug discovery, andrographolide is no exception. Andrographolide (AG), the primary diterpenoid compound, is responsible for the majority of its therapeutic effects. AG has a strong bitter taste and is responsible for most of the bioactivities of the plant, such as anti-viral, hepatoprotective, anti-cancer, anti-inflammatory, anti-arthritic, anti-diabetic, and anti-hyperlipidemic properties (Sinha & Raghuwanshi, 2000; Rajanna *et al.,* 2021; Jiang *et al.*, 2021).

Current research showed that AG provides a new option for pharmacological studies that might

lead to better approaches to treating a wide range of illnesses, including cancer, colitis, and Parkinson's (Lu *et al.,* 2019; Guo *et al.,* 2019; Khan *et al.,* 2021). Further clinical and experimental investigations are needed to accurately define the dosages, methods of intervention, and any adverse side effects. It is widely known that the failure rates in the clinical phase of drug discovery are high due to undesirable pharmacokinetics and toxicity of the drug candidate (Tuntland *et al.,* 2014). Therefore, analyzing absorption, distribution, metabolism, excretion and toxicity (ADMET) properties through *in silico* and *in vitro* approaches should be considered as early as possible because these tools are also essential for the prediction of *in vivo* pharmacokinetics (Dunninton *et al*., 2018). Hence, the current study attempted to confirm the preferred drug-like compound, AG using a standardized aqueous extract of *A. paniculata* through *in silico, in vitro,* and *in vivo* investigations. This study will offer information on the pharmacokinetic profiles of AG, which is critical not only for determining the proper dose regimen but also for reducing the likelihood of adverse effects due to overdose.

MATERIALS AND METHODS

ADMET prediction

ADMET parameters were predicted using ADMET Predictor® 9.5 (Simulations-Plus, Inc.) on a Windows XP operating system (Seyedhosseini *et al.,* 2022). The chemical structure of AG (Figure 1) was downloaded from the drug bank database in SMILES format. The structure was introduced into ADMET Predictor® 9.5 as: [H][C@]12CCC(=C)[C@@H](C\C=C3/[C@H](O)COC3=O)[C@]1(C)CC[C@@H](O)[C@@]2(C)CO. The simulated models used in this simulation were the physicochemical and biopharmaceutical (PhysChem), metabolism, and toxicity modules.

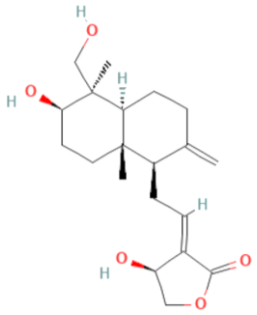

Figure 1. The chemical structure of Andrographolide (AG)

Chemicals

AG was obtained from Proliv Life Science Sdn. Bhd., Malaysia. Tween 80 and Nicotinamide adenine dinucleotide phosphate (NADPH) were purchased from Colorcon, India, and Sisco Research Laboratories, India, respectively. Dimethyl acetamide (DMA) and methyl cellulose were obtained from Merck, Germany, and hydroxy propyl beta cyclodextrin (HPßCD) was from Roquette, France. Phosphoric acid was purchased from Loba Chemie, India. Other chemicals were from Sigma–Aldrich, USA.

Preparation of *A. paniculata* aqueous extract

The leaves of *A. paniculata* were collected from Naturemedic Laboratories Sdn Bhd, Malaysia under the voucher specimen number, UniSZA/A/000000010. The extraction was done following the procedure described by Abubakar *et al.* (2020). The leaf sample was ground into powder. Then, the sample was extracted using a maceration process in filtered water at 60°C for 3h, followed by the spray drying process. The sample extract was kept at 4°C for the next test.

High-performance liquid chromatography (HPLC*)*

HPLC system consisted of a Waters 2690 Alliance Separation Module with Zorbax Eclipse XDB-C18 (4.6 mm × 150 mm × 5 µm) set to 280 nm and a computer system for data acquisition (Empower software, Waters) was used (Al Harthi *et al.,* 2015). About 100 mg of *A. paniculata* extract was dissolved into 25 mL of methanol. Then, the extract was vortexed and then filtered through a 0.45 µm nylon filter. Meanwhile, 1.0 mg of the standard was prepared by dissolving in 1 mL of 50% methanol and sonicated for 5 min. Mobile phases consisting of methanol (60%) and deionized water (40%) were employed at a flow rate of 1.0 mL/min (Ismail *et al.,* 2022).

Aqueous stability test

The positive standards, chlorambucil, and erythromycin were dissolved in dimethylsulfoxide (DMSO) to create stock solutions with a concentration of 10 mM (Yu *et al.,* 2018). For neutral pH, Dulbecco's phosphate buffer saline (DPBS) was adjusted to pH 7.4. Simulated gastric fluid was prepared by dissolving sodium chloride (150 mM) in 800 mL of distilled water and adjusted to pH 2. Sodium bicarbonate buffer was prepared for basic pH which was pH 9.2. The assay buffer was initially preincubated at 37 °C for 5 min.

Subsequently, 30 µL of the sample was introduced and allowed to incubate at 37°C for 120 min. Throughout this incubation period, 250 µL of the sample mixture was extracted at 0, 30, 60, and 120 minutes and transferred into tubes containing 250 µL of acetonitrile along with the internal standards (carbamazepine, furosemide, celecoxib, and telmisartan). Their robust stability across different pH conditions, serves as dependable references. Their well-understood degradation pathways also help in comparing the stability of other drugs. The samples were analyzed by LC-MS/MS API- 4000 (Shimadzu, Japan) coupled with an ACE 3 C18, 4.0 × 150 mm. The results were reported as the mean ± SD and the following equation was used to calculate aqueous stability:

$$\text{Aqueous stability} = \frac{\text{peak area of a compound at X hr}}{\text{peak ratio of a compound at 0 hr}} \times 100 \ldots\ldots\ldots\ldots(1)$$

Equilibrium solubility test

The solubility of AG was evaluated in DPBS with pH 7.4 in triplicates (Tang *et al.,* 2019). Briefly, the test and control compounds (estriol and propranolol HCl) were incubated in DMSO (200 µM) and DPBS (1 mg/mL) at 25 °C for 24 h. After incubation, the suspension was filtered through 0.45 µm syringe filters. Then, the AG compound was analyzed for dissolved content of the test substance in the filtrate by HPLC method (Waters, 2695) equipped with a Waters: Xterra, 4.6 × 150 mm, 5 µm column. The flow rate was set at 1.0 mL/min and the mobile phases were as follows:
A: Ammonium acetate: acetonitrile (90:10); B: Ammonium acetate: acetonitrile (5:95); C: Ammonium acetate: methanol (10:90); D: Methanol (100).

Meanwhile, 10 mM of DMSO stock solution was also prepared as a standard solution and calculated using the formula:

$$\text{Equilibrium solubility} = \frac{\text{Standard solution concentration} \times \text{peak area of a compound in PBS}}{\text{mean peak area of compound in 100\% DMSO}} \ldots\ldots(2)$$

***In vitro* plasma stability test**

The stability of AG was studied in the plasma of mouse, rat, dog, and human as described in the previous report (Konsoula & Jung, 2008). A total of 297 µL of plasma was preheated at 37 °C for 5 minutes in a shaking water bath. The reaction was initiated by introducing 3 µL of 1.0 mM AG and the positive control (enalapril), followed by an incubation period at 37°C for 120 min. At various time points (0, 30, 60, 90, and 120 min), 50 µL of samples were withdrawn and combined with 1.0 mL of ethyl acetate, which contained the internal standards (Celecoxib and Furosemide). Celecoxib and furosemide are widely accepted internal standards due to their well-characterized stability and behavior in plasma.

The plasma samples in ethyl acetate were thoroughly mixed by vortexing for 5 min and then subjected to centrifugation at 13,000 rpm for 10 minutes. The supernatant was removed, evaporated to dryness under nitrogen gas in vials, and reconstituted with 200 µL of water: acetonitrile (1:1) containing 0.1 % v/v formic acid. The supernatants were analyzed by LC-MS/MS. Plasma stability was calculated as the following equation:

$$\text{Plasma stability} = \frac{\text{peak area of a compound at X hr}}{\text{peak ratio of a compound at 0 hr}} \times 100 \ldots\ldots\ldots\ldots(3)$$

The samples were measured using an MDS-Sciex (Applied Biosystems) API 4000 Q-Trap mass spectrometer with an electrospray ionization source. Mass detection was performed in the negative ion mode. For multiple reaction monitoring (MRM) analyses, the target ions used were 349.2 ® 287 m/z. ACE 3 C18, 4.0 ´ 150 mm was used as the column. A flow rate at 1.0 mL/min was used with a gradient elution program: 0.01 min, 25% eluent A and 75% eluent B; 3.50 min, 25% eluent A and 75% eluent B. Eluent A consisted of formic acid and water. Eluent B consisted of acetonitrile.

***In vitro* permeability test**

Human intestinal adenoma-colon carcinoma (Caco-2) monolayer was employed in the test (Kamiya *et al.,* 2020). Caco-2 cells (American Type Culture Collection, USA) (Cat No. CRL-2102™) were cultured in Dulbecco's Modified Eagle's medium (DMEM), supplemented with 10% FBS, 1 mM sodium pyruvate, 1 mM non-essential amino acids, and 1% PS at 37 °C in an atmosphere of 5% CO_2 and 95% relative humidity. Caco-2 cells were seeded at 40,000 cells per insert into Millicell inserts and cultured for 21 days. Before treatment, the grown cells were rinsed with 1´ of Hank's Buffered Saline Solution (HBSS). Then, the monolayer integrity was checked using Trans Epithelial Electrical Resistance (TEER), with the accepted value of TEER of >320 ohm cm^2. Fresh working solutions (10 µM) were prepared for standard and test compounds by diluting in 1´ HBSS.

The permeability of the cell monolayer was measured from both the apical to the basolateral (AP to BL) and the basolateral to the apical (BL to AP) sides. For AP to BL, 0.3 mL of HBSS and 0.2 mL of the samples were added to all inserts. The inserts were then incubated for 1 h in a humidified chamber maintained at 37 °C. For BL to AP, 0.3 mL of 1× HBSS and 0.2 mL of the samples were added to all inserts and incubated for 40 min at 37 °C. After removing the plate from the humidified chamber, both apical and basolateral solutions were analyzed using LC-MS/MS API- 4000 (Shimadzu, Japan). Following the permeability assay, a Lucifer Yellow Rejection (LYR) test was performed to ensure monolayer integrity. Only cell monolayer inserts with a LYR of 98% were evaluated for the analysis. P_{app} values were calculated using the following equation.

$$\text{Papp } \left(\frac{cm}{sec}\right) = \frac{dQ}{dt} \times \frac{Vd}{C0} \times \frac{1}{A} \ldots\ldots\ldots\ldots(4)$$

where dQ/dt = permeability rate in μg/s
C_0 = initial concentration in μg/mL; A = membrane surface area (0.6 cm^2 for 12 mm inserts); V_d = volume in donor well (0.3 mL)

In vitro metabolic stability

In the liver microsomes of mice, rats, dogs, and humans, the metabolic stability of AG was determined (Bae *et al.,* 2020). A working stock solution containing 1.0 mM nicotinamide adenine dinucleotide phosphate (NADPH) and 4.0 M AG was made in potassium phosphate buffer. Incubation mixture containing pooled liver microsomal protein (55 μL), and AG (25 μL) in potassium phosphate buffer (pH 7.4) were preincubated at 37 °C for 5 min. For positive control, verapamil was used. To start the reaction, 20 μL of NADPH was added to all tubes except the T_0 tubes. The mixture was then incubated at 37 °C for 5, 15, and 30 min. For T_0, acetonitrile (internal standard) was added before mixing with pre-heated NADPH. At respective time intervals, the reaction was stopped with the addition of 100 μL of acetonitrile containing the internal standards (carbamazepine/celecoxib/furosemide/telmisartan). These internal standards were chosen due to their well-documented metabolic pathways, chemical stability, distinct analytical signals, and minimal interference with other compounds. Their use ensures accurate and reproducible results, providing a consistent reference point for evaluating the metabolic stability of the test compounds (Bae *et al.,* 2020).

The supernatant was then analyzed using LC-MS/MS, employing MDS-Sciex (Applied Biosystems) API 4000 Q-Trap mass spectrometer with an electrospray ionization source. Mass detection was performed in the negative ion mode. For MRM mode, the target ions used were 349.2 ® 287 m/z. The percentage of parents remained at the end of 30 minutes was calculated as shown below:

$$\text{Percentage of parent remained at } X \text{ time} = \left(\text{time X peak area ratio } \frac{time\ X\ peak\ area\ ratio}{T0\ peak\ area\ ratio}\right) \times 100 \ldots(5)$$

In vitro CYP450 isomers inhibition assay

The assay was conducted using a human liver microsome (Xenotech LLC, USA) (Lin *et al.,* 2007). In brief, 80 μL of microsomal protein was combined with 20 μL of each CYP450 isoform substrate. The assay mixture was then treated with 2 μL of andrographolide (1 and 10 M) and positive control (10 M). The solution was then pre-incubated for 5 min at 37 °C in a shaking water bath. A pre-incubated 100 μL solution containing 2.0 mM of NADPH was added to each tube. The reaction was stopped by adding 200 μL of quenching solution (acetonitrile with internal standard) to all tubes after 20 min of incubation. The samples were then analyzed with LC-MS/MS analysis. Changes in metabolite signal were monitored using electrospray ionization in the multiple reaction monitoring (MRM) mode on an Applied Biosystems MDS Sciex API-4000 Q-Trap (Toronto, Canada) for the LC/MS-based assay. Waters: Xterra, 4.6 ´ 50 mm, 3 μm was used as the column. For chromatographic conditions, a flow rate at 1.0 mL/min was used with a gradient elution program: 0.05% of formic acid in water for eluent A and 0.05% of formic acid in acetonitrile for eluent B. The run time was 6 min and the autosampler temperature was 5 °C. The following equation was used:

$$\%\ \text{Inhibition} = \left[100\ \left(\frac{mean\ test\ peak\ area\ ratio - mean\ blank\ area\ ratio}{mean\ control\ peak\ area\ ratio}\right) \times 100 \ldots(6)\right.$$

In vivo animal study

The ethical approval was obtained from the Animal Welfare Division, Ministry of Environment, Forest and Climate Change, India under the Animal License "812/PO/RcBi/S/04/CPCSEA". Male Wistar rats (245–265 g) used in the study were obtained from the in-house breeding facility at Auregene Pharmaceutical Services Limited, India. Six animals were housed in a cage (n = 3/cage) under controlled environmental conditions (26 ± 1 °C with 12-h light/dark cycles).

Rats were acclimatized to the experimental environment for 4 days before the experiment started. At the rates of 50 mg/kg and 5 mg/kg, AG was administered orally and sublingually (IV), respectively to three rats in each group. The AG compound was dissolved in Tween 80 and 0.5% w/v methyl cellulose for oral administration. Solution for intravenous (IV) was prepared using a mixture of 3% v/v dimethyl acetamide (DMA) and 10% w/v hydroxy propyl beta cyclodextrin (HPßCD).

Sample collection and analysis

Animals were euthanized by CO_2 overdose. Blood samples (0.13 mL) were collected at 0.25, 0.5, 1, 2, 4, 8, and 24 h for oral and 0.12, 0.25, 0.5, 1, 2, 4, 8, and 24 h for IV, in microcentrifuge tubes containing 15 µL of Di sodium ethylene diamine tetra acetic acid (Na_2EDTA). The plasma samples were preserved at -80 °C until examination, and quantitative bio-analysis was carried out through LC-MS/MS, employing an HPLC system, which consisted of a binary pump LC-20AD Prominence, a Degasser DGU-20A3 Prominence, an Autosampler SIL-HTC Prominence, and a Column Oven CTO-10 A Prominence (Shimadzu, Japan). On the other hand, for the mass spectrometer, we employed API-4000 instruments that were equipped with a Turboion Spray (AB Sciex, Canada). The analysis of the plasma samples involved protein precipitation using acetonitrile containing the internal standard (Celecoxib and Furosemide) and 0.15% v/v phosphoric acid. The lower limit of quantitation was set at 5 ng/mL.

Pharmacokinetic parameters for the plasma were computed by utilizing individual plasma concentration-versus-time profiles. This analysis was performed with the assistance of a non-compartmental analysis tool integrated into the Phoenix WinNonlin Professional software (Version 6.4.0, Pharsight Corporation, USA). Plasma pharmacokinetic parameters, including the area under the plasma concentration-time curve ($AUC_{0-\infty}$ and $AUC_{0\text{-last}}$), maximum concentration (C_{max}), time to reach C_{max} (T_{max}), initial concentration at 0 hours (C_0), elimination half-life ($T_{1/2}$), clearance (CL), and volume of distribution (V_{ss} and V_d), were derived from the plasma concentration-time profile. The absolute oral bioavailability was computed using the following formula:

Absolute oral bioavailability =

$$\frac{\text{AUC } oral \times \text{DOSE } iv}{\text{AUC } iv \times \text{DOSE } po} \times 100 \quad (7)$$

RESULTS AND DISCUSSION

In silico ADMET analysis was conducted based on computational modeling techniques to give an early insight into the ADMET profile of AG before pursuing *in vitro* and *in vivo* assays (Turner *et al.,* 2011). The predicted physicochemical properties demonstrated that AG satisfied Lipinski's rule of five, (MW < 500, logP < 5, HBD < 5, and HBA < 10), as well as Veber's rule (TPSA 140 < Å and Nrot < 10) indicating that this molecule has good absorption and likely good oral bioavailability (Table I).

The aqueous solubility of AG exceeded the Simulations-Plus suggested high-risk threshold of 0.01 mg/ml, showing that the compounds' solubility is comparable to orally bioavailable drugs (El-Saadi *et al.,* 2015). Meanwhile, a qualitative permeability model for BBB was predicted to have high permeability and therefore AG has a high chance of penetrating the blood-brain barrier and could be developed as a central nervous system drug for Alzheimer's disease (Morofuji & Nakagawa, 2020). *In silico* data of AG were compared with *in vitro* results and it exhibited similarities in terms of solubility, permeability, likelihood of BBB penetration, and intestinal efflux by p-glycoprotein (p-gp). The Peff and MDCK scores of AG were classified as a highly effective jejunal permeation with a low risk of low apparent permeation. Characterization of distribution PK profile such as drugs with a blood-to-plasma concentration ratio, human and rat plasma protein binding, volume of distribution, and fraction unbound in human liver microsomes of AG showed that these values were in the recommended range.

Distribution of AG was described based on the drug's capacity to pass from intravascular space, such as blood vessels, to extravascular areas, such as bodily tissues. AG avoided high RBC partitioning and extensive plasma protein regions in this study. This means that AG was not influenced by RBC metabolism and can approach the therapeutic target, which is a desirable feature of an effective drug (Kok-Yong & Lawrence, 2015). Compound liability of AG was also predicted using two models (ADMET_risk and Absn_risk) and it revealed that AG was a low-risk oral drug.Following that, the predicted metabolism properties include the CYP substrate/no substrate classification model and CYP inhibition for the major cytochrome P450s. The program also integrated the site of metabolism and kinetic predictions (K_m, V_{max}, and C_{Lint}) to generate maps of likely metabolites via the MedChem Designer™ auxiliary program.

Table I. Physicochemical analysis of AG based on in silico and in vitro experiments

Property	**Description**	**Recommended range**	***In silico* data of AG**	***In vitro* data of AG**
MW	Molecular weight g/mol	<450	350.45	NA
HBD	Number of hydrogen donor	<5	3	NA
HBA	Number of hydrogen acceptor	≤8	5	NA
Nrot	Number of rotatable bonds	<10	3	NA
TPSA	Topological polar surface area	<140 Å	86.99 Å	NA
MlogP	Moriguchi octanol to water partition coefficient	NA	1.801	NA
S+logP	Octanol to water partition coefficient	≤4.5	1.287	2.632 (Loureiro *et al.,* 2022)
S+logD	Octanol to water distribution coefficient	≤3.5	1.287	NA
S+Sw	Aqueous native solubility	≥0.010 mg/mL	1.184 mg/mL	High (152.17 ± 0.06 μM)
BBB_Filter	Qualitative likelihood of crossing the blood-brain barrier	High/Low	High (86%)	Yes (Gong *et al.,* 2022)
LogBB	Blood–brain partition coefficient	-1.0	-0.578	NA
Pgp_Substr	Intestinal efflux by P-gp transporter	Yes/No	Yes (94%)	Yes (2.0 of efflux ratio)
Pgp_Inh	Inhibition of the intestinal P-gp transporter	Yes/No	No (96%)	NA
S+Peff	Effective permeability	>0.5 cm/s × 10^4	1.904 cm/s × 10^4	Moderate, Apical: 9.627 × 10^{-6} cm/s Basolateral: 18.1 × 10^{-6} cm/s
S+MDCK	Apparent permeability	>30 cm/s × 10^7	159.504 cm/s × 10^7	NA
Perm_Skin	Skin permeability	NA	0.199 cm/s×10^7	Yes (Bayazid & Jang, 2021)
Perm_Cornea	Corneal permeability	NA	71.013 cm/s×10^7	Yes (Rozo *et al.,* 2022)
RBP	Blood-to-plasma concentration ratio	<1.0	0.82	NA
F_{up}	Percent of drug unbound to plasma proteins	>10%	34.54%	Not stable (<50%)
S_fumic	Fraction unbound in human liver microsomes	NA	0.868	Stable ($t_{1/2}$= >30 min)
V_d	Volume of distribution	≤3.7 L/kg	1.095 L/kg	NA
Absn_risk	Risk summary for oral absorption	<3.5	0	NA
ADMET_risk	Summary of all predicted ADMET risk factors	<6.5	2.131	NA

Table II. Toxicity analysis of AG based on *in silico*, *in vitro/in vivo* experiments

Property	**Description**	**Recommended range**	***In silico***	***In vitro/in vivo* data reported by other studies**
MRTD	Maximum recommended therapeutic dose in mg/kg/day	>3.16	Below >3.16	NA
Estro_filter	Estrogen receptor (rat)	Toxic/Non-toxic	Nontoxic (83%)	NA
Estro_RBA	Relative binding affinity	Toxic/Non-toxic	Nontoxic	NA
Sens_Skin	Skin sensitivity	Sensitizer/None	None	Rash (Ciampi *et al.,* 2020)
Sens_Resp	Respiratory sensitivity	Sensitizer/None	None	NA
Andro_filter	Androgen receptor (rat)	Toxic/non-toxic	Toxic (50%)	No testicular toxicity (Burgos *et al.,* 1997)
Andro_RBA	Relative binding affinity	Toxic/Non-toxic	0.002%	NA
hERG_pIC_{50}	hERG K+ channel	<5.5 M	4.185 M	No inhibition (Abdul Majid *et al.,* 2022)
Chrom_Aberr	Chromosomal aberration	Toxic/Non-toxic	Toxic	Nongenotoxic at 10-50 μM in both AHH-1 and MCL-5 cell lines (Sharifuddin *et al.,* 2012)
PLipidosis	Phopholipidosis	Toxic/Non-toxic	Nontoxic	NA
Rat_Acute_LD50	Lethal acute rat toxicity	NA	127.95 mg/kg	> 5000 mg/kg BW (Worasuttayangkurn *et al.,* 2019)
Rat_TD_{50}	Carcinogenicity in rat	>4 mg/kg/day	14.64 mg/kg/day	NA
Mouse_TD_{50}	Carcinogenicity in mouse	>25 mg/kg/day	440.48 mg/kg/day	NA
Repro_Tox	Reproductive toxicity	Toxic/Non-toxic	Toxic (76%)	Toxic (Huang *et al.,* 2019)
Ser_AlkPhos	Level of alkaline phosphate enzyme	Elevated/normal	Elevated (64%)	NA
Ser_GGT	Level of GGT enzyme	Elevated/normal	Normal (86%)	Noncytotoxic against HepG2 cell line (Sa-ngiamsuntorn *et al.,* 2021)
Ser_LDH	Level of LDH enzyme	Elevated/normal	Elevated (63%)	NA
Ser_ ALT	Level of ALT enzyme	Elevated/normal	Elevated (89%)	NA
MUT_Risk	Risk summary for mutagenic potential in *S. typhimurium*	≤1	0	Nonmutagenic (Srinivasan *et al.,* 2021)
TOX_Risk	Overall toxicity risk	1	2	NA

The result showed that AG inhibited all the isoforms (Supplementary 1). AG was also non-substrate to all CYP isoforms except for CYP3A4 (83%). The predicted K_m, V_{max}, and C_{Lint} for CYP3A4 were 183.298, 77.772, and 47.096, respectively. The site of metabolism for CYP3A4 was predicted as in Supplementary 2. The CYP risk was 2.131.

Next, AG was assessed to determine its likelihood of being toxic, allergenic, and mutagenic (Table II). Through the MRTD module, a potential for side effects for AG was predicted as the value was lower than 3.16 mg/kg-bw/day and the value of hERG_pIC_{50} was less than 5.5 M, indicating that human ether-a-go-go-related (hERG) gene was not suppressed. The AG compound was also not a skin or respiratory sensitizer. Furthermore, phospholipidosis was discovered to be non-toxic. However, AG was predicted to bind detectably to the androgen receptor with a 0.002% degree of binding affinity. Although the AG compound was shown to be non-toxic to estrogen, it is likely to bind to the androgen receptor, which suggests the possibility that it could interfere with the normal transmission of hormonal signals and be potentially harmful. Predictions for reproductive and chromosomal aberration were also found to be toxic. Therefore *in vitro* genotoxicity study must be done to verify the finding. The predicted reproductive toxicity of AG was supported by *in vivo* findings from previous studies (Liang *et al.,* 2018). They discovered that after sperm injection, AG disrupted the spindle tissue and migration, as well as inhibited oocyte development in mice. Increased levels of ALT and LDH enzymes, as well as Ser AlkPhos or Ser GGT, were observed. Only the Ser GGT level was within the normal level. Finally, AG had no mutagenic effect but had a value of 2 for overall toxicity.

To detect and quantify AG in *A. paniculata*, HPLC analysis was performed. As shown in Supplementary 3, the extract was compared with the standard and the result showed that AG produced the highest content of phytochemical with a concentration of 5.295 ppm at 3.181 min.

The aqueous stability of AG was assessed in different pH levels and based on classification criteria, the percent parent remained at 60 min with >70 being considered as stable, 50–70 being moderately stable, and <50 being classified as unstable. AG remained stable for 120 min at pH 2.0 (90%), pH 7.4 (95.60%), and pH 9.2 (83.70%). The previous study revealed that the stability of AG varied in different pH with the best condition of pH 3-5 (Yan *et al.,* 2018).

For the solubility test, based on the assessment criteria, the mean solubility of >100 μM is considered highly soluble. In this study, AG was regarded as a highly soluble compound with 152.17 ± 0.06 μM of mean solubility in DPBS after 24 h. Estriol and propranolol have mean solubilities at 66 μM and >200 μM, respectively. These controls were chosen in this study because their solubilities in various solvents are well established and therefore provide a reliable baseline for validating the solubility test. Meanwhile, for the plasma stability test, AG was moderately stable in mouse but unstable in rat, dog and human plasma with less than 50% of the parent remaining after 120 min.

Caco-2 cell line was used as a reliable model to examine how drugs are absorbed through the intestine and the related processes involved (Kamiya *et al.,* 2020). A compound that was entirely absorbed in the intestine had a high permeability coefficient (P_{app} AP to BL > 1×10^{-6}) but an incompletely absorbed medication had a low permeability coefficient (P_{app} AP to BL 1×10^{-7}). Permeability AG was found to be moderately permeable with a P_{app} value of 9.627×10^{-6} cm/s for the apical and 18.1×10^{-6} cm/s for basolateral directions. The estimated efflux ratio was 2.00, which suggests that compounds might be a substrate of efflux transports including p-glycoprotein.

Since there are many drug-metabolizing enzymes found in the liver, subcellular fractions like liver microsomes are ideal *in vitro* models of hepatic clearance (Bae *et al.,* 2020). Evaluating the PK profile that underlies dosage and dose frequency requires understanding the metabolic stability of the drug candidates eliminated by metabolism (Knights *et al.,* 2016). AG was exposed to liver microsomes of four species to determine the interspecies variation of microsomal stability. However, only the microsomal half-life of mouse was calculated at more than 30 min, indicating that other microsomes might not be stable to oxidative metabolism in the liver.

CYP3A4 is involved in the majority of drug metabolism (Lin *et al.,* 2007). Other important CYP450 enzymes include CYP1A2, CYP2C9, CYP2C19, and CYP2D6. In the present study, AG did not inhibit the activities catalyzed by CYP2C8, CYP19, CYP2D6, and CYP3A4 (MDZ) (Supplementary 4). This result matched the findings of *in silico* ADMET. However, for CYP1A2, it was noted a contradictory result for this enzyme.

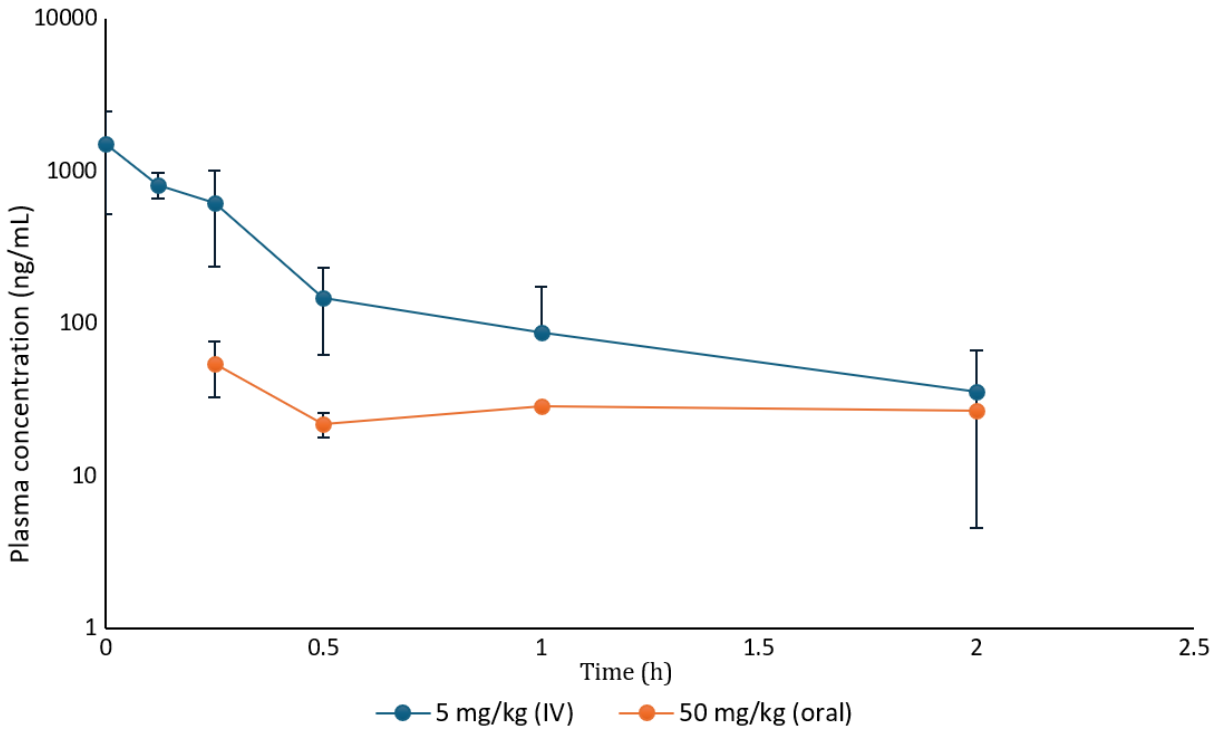

Figure 2. Mean plasma concentration vs time profiles of AG at 5 mg/kg intravenous (IV) and 50 mg/kg oral and dose in male Wistar rats. Values represent the mean and standard deviation (SD) (n= 3).

Table III. Mean values of pharmacokinetic parameters for AG when compared to the previous reports. Values represent the mean and standard deviation (SD) (n= 3).

Parameter	**AG**		**(Yang *et al.*, 2013)**	**(Bera *et al.*, 2013)**
Route of administration	**IV**	**Oral**	**IV**	**Oral**
Dosing	5 mg/kg	50 mg/kg	5 mg/kg	100 mg/kg
Area under curve (0 to last time measured) ($AUC_{0\text{-}last}$)	390±45.65 ng*h/mL	66±29.10 ng*h/mL	NA	259.16 ± 32.68 ng*h/mL
Peak plasma concentration (C_{max})	NA	73±40.90 ng/mL	NA	115.81 ± 17.56 µg/mL
Time to reach C_{max} (T_{max})	NA	0.25±0.0h	NA	0.75 ± 0.29 h
Initial plasma concentration (C_0)	1515±984 ng/mL	NA	NA	NA
Elimination half-life ($T_{1/2}$)	0.17±0.0 h	NA	0.23±9.54 h	2.45 ± 0.44 h
Clearance (CL)	199±16.97 mL/min/kg	NA	94.99±29.02 mL/min/kg	NA
Volume of distribution (steady state) (V_{ss})	2.98±0.30 L/kg	NA	NA	NA
Volume of distribution (elimination) (V_d)	3.20±0.54 L/kg	NA	53.64±16.34 L/kg	NA
Mean resident time, (MRT_{last})	0.26±0.23 h	0.98±0.10h	7.35±102.73 h	NA
Oral bioavailability (F)	NA	1.69%	NA	2.67%

NA= Not applicable

The *in vitro* result showed a mild inhibition which was <10%, while the *in silico* result showed no inhibition. AG also showed moderate inhibition against the activities of CYP2B6, CYP2C9, and CYP3A4 (testo). These results also align with earlier research, providing more evidence that exposure to AG may have an impact on the activity of CYP inhibitors, in particular by inhibitors of CYP2B6 and CYP3A4 (testo) and potentially affecting the safety or efficacy of AG (Pan *et al.,* 2011). Another report also revealed that AG might affect warfarin metabolism in the rat liver by decreasing the activity of CYP2C9 and CYP3A4 (Zhang *et al.,* 2018). Hence, AG may cause herb-drug interactions, therefore is not recommended to be taken with the drugs metabolized by CYP1A2, CYP2B6, CYP2C9, and CYP3A4.

AG was further evaluated for *in vivo* animal study. The plasma concentration versus time profile of AG (Figure 2), while PK parameters (Table III) comparing with the *in vivo* results of andrographolide in the previous studies. The graph could not be depicted for 24 h because the plasma concentrations above two hours were below the lower limit of quantification. CL and V_{ss} are two factors that affect the elimination half-life of the compound (Jang *et al.,* 2001). CL value was found high in the present study, indicating that the drug was eliminated from the body at a rapid pace, and a drug with a high V_d suggests that it was distributed in tissues rather than binding to plasma or being distributed in blood. V_d was measured slightly higher than the *in silico* data reported in the current study (1.095 L/kg). In the previous study, other researchers reported a lower value of V_d which was 0.27 L/kg with 1 mg/kg of dosing through an intravenous route (Panossian *et al.,* 2000). In the study done by the previous researchers, they found a higher C_{max} of 115 ng/mL at 0.75 h post dose with elimination half-life of 2.45 h, following an oral administration of andrographolide in a dose of 100 mg/kg/day (Bera *et al.,* 2013). C_{max} value in the present study was lower which was 73.0 ng/mL, reaching 0.25 h with an elimination half-life of 0.17 h. AUC is inversely correlated to drug clearance. In other words, when clearance is higher, the drug remains in systemic circulation for a shorter duration, resulting in a more rapid reduction in plasma drug concentration. Therefore, AG in the present study has a faster rate of clearance, easily excreted from the body, and therefore contributed to its low bioavailability.

A group of researchers stated in their report that a drug's high clearance and short half-life are induced by rapid liver metabolism and excretion (Masimirembwa *et al.,* 2012). Panossian *et al.* (2000) and Ye *et al*. (2011) also reported low bioavailability values, which were 0.21% and 2.67%, respectively. The poor *in vivo* performance could also be related to the poor plasma stability of AG as observed in the *in vitro* study (Yuan *et al.,* 2022). Other than that, the contradiction of the findings from *in vitro* and *in vivo* studies may be due to the different solvents used to dissolve the compound. However, according to the earlier report, they found 2.67% of oral bioavailability of AG and they concluded that it was because of its fast metabolism and p-gp's affinity for efflux (Ye *et al.,* 2011).

CONCLUSION

In silico ADMET showed that AG was predicted to have good drug-like properties with adequate metabolic and toxicity profiles. Lipinski's rule of five was complied with no violation. AG also possessed a high potential for drug development based on desirable predicted aqueous solubility and optimum permeation values. This is in parallel with *in vitro* results which show a high stability in gastrointestinal neutral, alkaline, and acidic environments, high equilibrium solubility, and moderate absorption of intestinal permeability. Additionally, AG was classified as a lipophilic, non-mutagenic, and non-carcinogenic molecule and most likely to penetrate the BBB. Despite showing high metabolic stability in the microsomal extract of mouse, rat, dog, and human, AG did not inhibit the activity of CYP2C8, CYP2C19 CYP2D6, and CYP3A4 (MDZ). Based on *in vivo* PK parameters, it was concluded that AG was widely distributed and rapidly eliminated from the body and therefore contributed to its low oral bioavailability. The study confirmed the promising PK profile of AG, and together with its well-documented potent pharmacological features, this molecule is a promising lead candidate for a low-risk oral herbal drug against a wide range of illnesses.

ACKNOWLEDGMENTS

The authors would like to thank Naturemedic Laboratories, Terengganu, Malaysia for providing the raw material and Aurigene Discovery Technologies, Ltd., India for assisting in data analysis. This research was funded by NKEA Research Grant Scheme (NRGS), Ministry of Agriculture & Food Industries, Malaysia.

REFERENCES

Abdul Majid, F. A., Fadhlina, A., Ismail, H. F., Zainol, S. N., Mamillapalli, A. K., Venkatesan V., Eswarappa, R., & Pillai, R. (2022). Mutagenicity and safety pharmacology of a standardized antidiabetic polyherbal formulation. *Scientific Reports*, *12*, 7127. doi.org/10.1038/s41598-022-11243-3

Abubakar, A. R., Haque, M. (2020). Preparation of medicinal plants: basic extraction and fractionation procedures for experimental purposes. *Journal of Pharmacy and Bioallied Sciences*, *12*, 1-10. doi.org/10.4103/jpbs.JPBS_175_19

Al Harthi, S. S., Mavazhe, A., Al Mahroqi, H., Khan, S. A. (2015). Quantification of phenolic compounds, evaluation of physicochemical properties and antioxidant activity of four date (*Phoenix dactylifera* L.) varieties of Oman. *Journal of Taibah University Medical Sciences*, *10*, 346-352.

Bae, I. Y., Choi, M. S., Ji, Y. S., Yoo, S. K., Kim, K., Yoo, H. H. (2020). Species differences in stereoselective pharmacokinetics of HSG4112, a new anti-obesity agent. *Pharmaceutics, 12*, 127. doi.org/10.3390/pharmaceutics12020127

Bayazid, A. B., Jang, Y. A. (2021). The role of andrographolide on skin inflammations and modulation of skin barrier functions in human keratinocyte. *Biotechnology and Bioprocess Engineering, 26*, 804–813. doi.org/10.1007/s12257-020-0289-x

Bera, R., Ahmed, S. K., Sarkar, L., Sen, T., Karmakar, S. (2013). Pharmacokinetic analysis and tissue distribution of andrographolide in rat by a validated LC-MS/MS method. *Pharmaceutical Biology*, *52*, 321–329.

Burgos, R. A., Caballeroa, E. E., Sánchez, N. S., Schroeder, R. A., Wikman, G. K., & Hancke, J. L. (1997). Testicular toxicity assessment of *Andrographis paniculata* dried extract in rats. *Journal of Ethnopharmacology, 58*, 219-24.

Ciampi, E., Uribe-San-Martin, R., Cárcamo, C., Cruz, J.P., Reyes, A., Reyes, D. et al. (2020). Efficacy of andrographolide in not active progressive multiple sclerosis: a prospective exploratory double-blind, parallel-group, randomized, placebo-controlled trial. *BMC Neurology*, *20*, 173. doi.org/10.1186/s12883-020-01745-w

Dunnington, K., Benrimoh, N., Brandquist, C., Cardillo-Marricco, N., Spirito, M. D., Grenier, J. (2018). Application of pharmacokinetics in early drug development. in (ed.), pharmacokinetics and adverse effects of drugs - mechanisms and risks factors. *IntechOpen* doi.org/10.5772/intechopen.74189

El-Saadi, M. W., Williams-Hart, T., Salvatore, B. A., Mahdavian, E. (2015). Use of in-silico assays to characterize the ADMET profile and identify potential therapeutic targets of fusarochromanone, a novel anti-cancer agent. *In Silico Pharmacology, 3*, 6. doi:10.1186/s40203-015-0010-5

Gong, P., Zhang, W., Zou, C., Han, S,. Tian, Q., Wang, J. et al. (2022). Andrographolide attenuates blood-brain barrier disruption, neuronal apoptosis, and oxidative stress through activation of nrf2/ho-1 signalling pathway in subarachnoid hemorrhage. *Neurotoxicity Research, 40,* 508–519. doi.org/10.1007/s12640-022-00486-7

Guo, B. J., Liu, Z., Ding, M. Y., Li, F., Jing, M., Xu, L. P. et al. (2019). Andrographolide derivative ameliorates dextran sulfate sodium-induced experimental colitis in mice. *Biochemical Pharmacology*, *163*, 416-24.

Huang, H., Cao, H., Xing, C., Hua, Y., Zhang, M., Jin, L. (2019). Andrographolide induce human embryonic stem cell apoptosis by oxidative stress response. *Molecular Cell Toxicology, 15*, 209–219. doi.org/10.1007/s13273-019-0024-x

Ibrahim, N. D., Seow, L.J., Sekar, M., Rani, N. N. I. M., Lum, P. T. (2020). Ten commonly available medicinal plants in malaysia with potential sun protection factor and antioxidant properties – a review. *Pharmacognosy Journal*, *14*, 444-455.

Ismail, H. F., Fadhlina, A., Zainol, S. N., Mamillapalli, A. K., Venkatesan, V., Eswarappa, R., Pillai, R., & Majid, F. A. A. (2022). Favourable drug-lead pharmacokinetic features for designing gallic acid-standardized *Syzygium polyanthum* aqueous extract-based product. *Indonesian Journal of Pharmacy*, *33*(4), 666–679. https://doi.org/10.22146/ijp.3639

Jang, G. R., Harris, R. Z., Lau, D. T. (2001). Pharmacokinetics and its role in small molecule drug discovery research. *Medicinal Research Reviews, 21*, 382-396. doi:10.1002/med.1015

Jiang, M., Sheng, F., Zhang, Z., Ma, X., Gao, T., Fu, C. et al. (2021). *Andrographis paniculata* (Burm.f.) Nees and its major constituent

andrographolide as potential antiviral agents. *Journal of Ethnopharmacology, 272,* 113954. doi:10.1016/j.jep.2021.113954

Kamiya, Y., Takaku, H., Yamada, R., Akase, C., Abe, Y., Sekiguchi, Y. et al. (2020). Determination and prediction of permeability across intestinal epithelial cell monolayer of a diverse range of industrial chemicals/drugs for estimation of oral absorption as a putative marker of hepatotoxicity. *Toxicology Report, 7*, 149-154. http://doi:10.1016/j.toxrep.2020.01.004

Khan, I., Mahfooz, S., Saeed, M., Ahmad, I., Ansari, I. A. (2021). Andrographolide inhibits proliferation of colon cancer sw-480 cells via downregulating notch signalling pathway. *Anticancer Agents in Medicinal Chemistry, 21*, 487-97.

Knights, K. M., Stresser, D. M., Miners, J. O., Crespi, C. L. (2016). In vitro drug metabolism using liver microsomes. *Current Protocols in Pharmacology,* 74, 7.8.1–7.8.24. doi.org/10.1002/cpph.9

Kok-Yong, S., Lawrence, L. (2015). Drug distribution and drug elimination. in (ed.), basic pharmacokinetic concepts and some clinical applications. *IntechOpen.* doi.org/10.5772/59929

Konsoula, R., Jung, M. (2008). In vitro plasma stability, permeability and solubility of mercaptoacetamide histone deacetylase inhibitors. *International Journal Pharmacy, 361*, 19–25. doi.org/10.1016/j.ijpharm.2008.05.001

Liang, E., Liu, X., Du, Z., Yang, R., Zhao, Y. (2018). Andrographolide ameliorates diabetic cardiomyopathy in mice by blockage of oxidative damage and nf-κb-mediated inflammation. *Oxidative Medicine and Cell Longevity,* 9086747. https://doi.org/10.1155/2018/9086747

Lin, T., Pan, K., Mordenti, J., Pan, L. (2007). In vitro assessment of cytochrome P450 inhibition: strategies for increasing LC/MS-based assay throughput using a one-point IC(50) method and multiplexing high-performance liquid chromatography. *Journal of Pharmaceutical Science, 96,* 2485–2493. doi.org/10.1002/jps.20884

Loureiro Damasceno, J. P., Silva da Rosa, H., Silva de Araújo, L., Jacometti Cardoso Furtado, N.A. (2022). *Andrographis paniculata* formulations: impact on diterpene lactone oral bioavailability. *European Journal of Drug Metabolism and Pharmacokinetics, 47*, 19–30. doi.org/10.1007/s13318-021-00736-7

Lu, J., Ma, Y., Wu, J., Huang, H., Wang, X., Chen, Z. et al. (2019). A review for the neuroprotective effects of andrographolide in the central nervous system. *Biomedicine & Pharmacotherapy, 117*, 109078.

Masimirembwa, C., Thelingwani, R. (2012). Application of in silico, in vitro and in vivo admet/pk platforms in drug discovery. In: Chibale, K., Davies-Coleman, M., Masimirembwa, C. (eds) Drug discovery in Africa. Berlin, Heidelberg: Springer, pp. 151-191. doi.org/10.1007/978-3-642-28175-4_7

Morofuji, Y., Nakagawa, S. (2020). Drug development for central nervous system diseases using in vitro blood-brain barrier models and drug repositioning. *Current Pharmaceutical Design, 26*, 1466-1485.doi:10.2174/1381612826666200224112534

Nugroho, A. E., Lindawati, N.Y., Herlyanti, K., Widyastuti, L., Pramono, S. (2013). Anti-diabetic effect of a combination of andrographolide-enriched extract of *Andrographis paniculata* (Burm f.) Nees and asiaticoside-enriched extract of *Centella asiatica* L. in high fructose-fat fed rats. *Indian Journal of Experimental Biology, 51*, 1101–1108.

Pan, Y., Abd-Rashid, B. A., Ismail, Z., Ismail, R., Mak, J. W., Pook, P. C. et al. (2011). In vitro determination of the effect of *Andrographis paniculata* extracts and andrographolide on human hepatic cytochrome P450 activities. *Journal of Natural Medicine, 65*, 440-447. doi:10.1007/s11418-011-0516-z

Panossian, A., Hovhannisyan, A., Mamikonyan, G., Abrahamian, H., Hambardzumyan, E., Gabrielian, E. et al. (2000). Pharmacokinetic and oral bioavailability of andrographolide from *Andrographis paniculata* fixed combination Kan Jang in rats and human. *Phytomedicine, 7,* 351–364. doi.org/10.1016/S0944-7113(00)80054-9

Rajanna, M., Bharathi, B., Shivakumar, B. R., Deepak, M., Prashanth, D., Prabakaran, D. et al. (2021). Immunomodulatory effects of *Andrographis paniculata* extract in healthy adults - An open-label study. *Journal of Ayurveda and Integrative Medicine, 12*(3), 529-534. doi: 10.1016/j.jaim.2021.06.004.

Rozo, V., Quan, M., Aung, T., Kang, J., Thomasy, S.M., Leonard, B.C. (2022). Andrographolide inhibits corneal fibroblast to myofibroblast differentiation in vitro. *Biomolecules, 12*, 1447. doi.org/10.3390/biom12101447

Sa-ngiamsuntorn, K., Suksatu, A., Pewkliang, Y., Thongsri, P., Kanjanasirirat, P., Manopwisedjaroen, S. et al. (2021). Anti-SARS-CoV-2 activity of *andrographis paniculata* extract and its major component andrographolide in human lung epithelial cells and cytotoxicity evaluation in major organ cell representatives. *Journal of Natural Product, 84*, 1261-1270. doi.org/10.1021/acs.jnatprod.0c01324

Seyedhosseini, G. H., Damavandi, M.S., Sadeghi, P., Massah, A. R., Hamidi Asl, T., Salari-Jazi, A. et al. (2022). Targeting and ultrabroad insight into molecular basis of Resistance-nodulation-cell division efflux pumps. *Scientific Report, 12*, 16130. doi.org/10.1038/s41598-022-20278-5

Sharifuddin, Y., Parry, E. M., Parry, J. M. (2012). The genotoxicity and cytotoxicity assessments of andrographolide in vitro. *Food and Chemical Toxicology, 50*, 1393–1398. doi.org/10.1016/j.fct.2012.01.039

Sinha, S. (2000). Raghuwanshi R. Evaluation of phytochemical, antioxidant and reducing activity in whole plant extract of *Andrographis paniculata* (Burm.f.) Wall. Ex Nees. *Bioscience Biotechnology Research Communi cations, 13*, 1734-1742.

Srinivasan, M. R., Preetha, S. P., Sudhakar, G. V., Tirumurugaan, K. G., Seshiah, A., Ramesh, S. (2021). Genotoxicity assessment of andrographolide in Ames mutagenicity assay and in vitro chromosomal aberration assay. *Pharma Innovation, 10,* 61-65.

Tang, J., Huber, A. D., Pineda, D. L., Boschert, K. N., Wolf, J. J., Kankanala, et al. (2019). 5-Aminothiophene-2,4-dicarboxamide analogues as hepatitis B virus capsid assembly effectors. *European Journal of Medicinal Chemistry, 164*, 179-192. doi:10.1016/j.ejmech.2018.12.047

Tuntland, T., Ethell, B., Kosaka, T., Blasco, F., Zang, R. X., Jain, M. et al. (2014). Implementation of pharmacokinetic and pharmacodynamic strategies in early research phases of drug discovery and development at Novartis Institute of Biomedical Research. *Frontier Pharmacology, 5*, 174. doi.org/10.3389/fphar.2014.00174

Turner, P. V., Brabb, T., Pekow, C., Vasbinder, M. A. (2011). Administration of substances to laboratory animals: routes of administration and factors to consider. *Journal of the American Association for Laboratory Animal Science, 50*(5), 600-613.

Worasuttayangkurn, L., Nakareangrit, W., Kwangjai, J., Sritangos, P., Pholphana, N., Watcharasit, P. et al. (2019). Acute oral toxicity evaluation of *Andrographis paniculata*-standardized first true leaf ethanolic extract. *Toxicology Reports, 6*, 426–430. doi.org/10.1016/j.toxrep.2019.05.003

Yan, Y., Fang, L. H., Du, G. H. (2018). Andrographolide. in: natural small molecule drugs from plants. Singapore: Springer, pp. 357-362.doi.org/10.1007/978-981-10-8022-7_60

Yang, T., Xu, C., Wang, Z. T., Wang, C. H. (2013). Comparative pharmacokinetic studies of andrographolide and its metabolite of 14-deoxy-12-hydroxy-andrographolide in rat by ultra-performance liquid chromatography-mass spectrometry. *Biomedical Chromatography*, *27*(7), 931–937. doi.org/10.1002/bmc.288

Ye, L., Wang, T., Tang, L., Liu, W., Yang, Z., Zhou, J. et al. (2011). Poor oral bioavailability of a promising anticancer agent andrographolide is due to extensive metabolism and efflux by P-glycoprotein. *Journal of Pharmaceutical Sciences, 100*(11), 5007-50017.

Yoopan, N., Thisoda, P., Rangkadilok, N., Sahasitiwat, S., Pholphana, N., Ruchirawat, S. et al. (2007). Cardiovascular effects of 14-deoxy-11,12-didehydroandrographolide and *Andrographis paniculata* extracts. *Planta Medica, 73*(6), 503–511. https://doi.org/10.1055/s-2007-967181

Yu, H., Yang, J., Ding, J., He, Y., Jiang, Z., Chai, X. et al. (2018). Stability study and identification of degradation products of caffeoylgluconic acid derivatives from *Fructus euodiae*. *Molecules, 23*(8), 1975. doi:10.3390/molecules23081975

Yuan, Y., Meng, G., Li, Y., Wu, C. (2022). Study on in vitro metabolism and in vivo pharmacokinetics of beauvericin. *Toxins*, 14, 477.

Zhang, X., Zhang, X., Wang, X., Zhao, M. (2018). Influence of andrographolide on the pharmacokinetics of warfarin in rats. *Pharmaceutical Biology*, *56*(1), 351–356. doi.org/10.1080/13880209.2018.1478431